Applied Radiation and Isotopes 212 (2024) 111419

Contents lists available at ScienceDirect

Applied Radiation and Isotopes

journal homepage: www.elsevier.com/locate/apradiso

Carbon-based thin films as a suitable alternative to metallized films for the preparation of radioactive sources

Rodolfo Fernández-Martínez [a,*], Mª Isabel Rodríguez-Tapiador [a], Miguel Roteta [a], María Pérez-Cadenas [c], Gilberto del Rosario [b], Jorge Pedrós [d], Isabel Rucandio [a]

[a] Centro de Investigaciones Energéticas, Medioambientales y Tecnológicas (CIEMAT) (Spain), Av. Complutense 40, Madrid, 28040, Spain
[b] Universidad Rey Juan Carlos, Calle Tulipán S/n, 28933, Móstoles, Madrid, Spain
[c] Dept. Química Inorgánica y Química Técnica, Facultad de Ciencias, UNED, Av. Esparta S/n, Las Rozas, 28232, Madrid, Spain
[d] Instituto de Sistemas Optoeléctronicos y Microtecnología & Departamento de Ingeniería Electrónica, E.T.S.I. de Telecomunicación, Universidad Politécnica de Madrid, Av. Complutense 30, Madrid, 28040, Spain

ARTICLE INFO

Keywords:
Graphene
Carbon nanotubes
Radioactive source
Source preparation

ABSTRACT

A new method for radionuclide labeling by the use of graphene thin films was previously presented. In this work, a comparison among low energy radioactive sources supported on carbonaceous thin films on polyvinyl chloride-polyvinyl acetate copolymer (VYNS), based on the use of aqueous solutions is investigated as a feasible alternative to the traditional metallized films avoiding the downside of the loss of many broken films. Graphene-based materials were prepared by both oxidation-exfoliation-reduction and direct graphite exfoliation routes. In addition, multiwalled carbon nanotubes (MWCNTs) thin films were also evaluated. The stability of both carbonaceous materials aqueous dispersions were studied by using ionic and non-ionic surfactants. Solid carbon-based materials were characterized by X-Ray Diffraction (XRD) and Fourier Transform Infrared Spectroscopy (FTIR) whereas the colloidal nature of the aqueous dispersions was verified by the measurement of Tyndall effect and the morphology of thin films was evaluated by Scanning Electron Microscopy (SEM). ^{55}Fe solutions were used to prepare the radioactive sources on the thin films by quantitative drop deposition. The quality of spectra was measured in a pressurized proportional counter. Results showed a resolution higher than 0.9 keV for all the tested sources. However, MWCNT-based along with non-surfactant sources presented non-adequate escape peaks and low energy tails. On the contrary, all the graphene-based sources prepared using surfactants to stabilize aqueous solutions presented an energy resolution comparable to that of the metallized source while offering notable advantages in terms of cost efficiency and reliability of the as-prepared supports.

1. Introduction

The preparation of good conductive sources is essential to obtain high quality electron spectra, especially if they are of low energy. The preparation of radioactive sources requires thin-film supports allowing radiation to pass through. The thin-film membrane can be made of a wide variety of materials such as polypyrrole and polyaniline films, polyethylene dioxythiophene/polyvinylchloride and polyvinylchloride-polyvinylacetate copolymer (VYNS) (deSanoit et al., 1997; Du et al., 1996; Sibbens and Altzitzoglou, 2007). All of them present common features that make them feasible for the application of the 4πγ method, including a very low surface density and a low average atomic number in order to reduce absorption and dispersion of radiation, tensile strength to resist the impact of drops of radioactive solutions poured from pipettes, chemical inertness to the reagents used during the rapid evaporation of solutions and thermal resistance to the infrared radiation used during the evaporation process and during the subsequent metallization process to make the film electrically conductive (Moura and Parker, 1975). Among them, VYNS is largely the most used material to prepare thin films for radioactive sources. Commonly, VYNS membranes are stretched on stainless steel or aluminum rings. The thickness of the thin film is determined by the concentration of VYNS in the solution., This ranges from several hundreds of μg cm^{-2}, although, is usually limited to 5–10 μm cm^{-2}. The thickness of the VYNS thin films may be measured gravimetrically. The evaporation of gold or gold-palladium thin layers onto VYNS allow becoming it into conductor. (Lowenthal, 1964). The

* Corresponding author.
E-mail address: rodolfo.fernandez@ciemat.es (R. Fernández-Martínez).

https://doi.org/10.1016/j.apradiso.2024.111419
Received 21 December 2021; Received in revised form 17 June 2024; Accepted 25 June 2024
Available online 4 July 2024

thickness of the conductive layer may be determined by the difference between the weight of the thin film with and without the conductive layer. The use of gold as conductive metal is related to its easy preparation, its excellent resistant to oxidation and chemical attack and its low migration rate at room temperature, which prevents the loss of the conductive nature of the deposited film (Yaffe, 1962). On the contrary, VYNS thin films are not resistant to the most commonly used organic solvents such as Dimethylformamide (DMF), *N*-methyl-2-pyrrolidone (NMP) or Dimethyl sulfoxide (DMSO).

This preparation method present several disadvantages, such as the cost of gold-palladium (Au–Pd) solutions and the fragility of the thin film when is coated with the metal, being common the breakage of a high proportion of them.

Carbonaceous materials, such as carbon nanotubes or graphene-based materials are appealing candidates to enable conductive films because of their good electrical conductivity, high tensile strength and excellent elasticity. MWCNTs are fiber-like engineered nanomaterials (ENMs) derived of both carbon fibers and fullerene with molecules composed of carbons in a rolled structure with an arrangement similar to graphite (Sonkar et al., 2021). MWCNTs are made of carbon sp2 forming van der Waals crystalline structures (Liu et al., 2018). Graphene is an allotropic form of carbon that has attracted great attention since Novoselov and Geim obtained sheets of graphene by exfoliating graphite using an adhesive tape in 2004 (Novoselov et al., 2004), a discovery by which they were awarded the 2010 Nobel Prize in Physics. Structurally, graphene consists of a single layer of carbon atoms tightly bonded by bonds that exhibit sp^2 hybridization and arranged in a uniform, slightly wavy surface, with a honeycomb structure due to its hexagonal electronic configuration. Graphene can be classified into three types: monolayer, bilayer and multilayer with a thickness between 3 and 10 layers (Geim and Novoselov, 2007). When the material present more than 10 layers its characteristics are similar to graphite. The properties of monolayer graphene are excellent, including its transparency (Nair et al., 2008), its high thermal conductivity (5300 W m^{-1} K^{-1}) (Balandin, 2011), the Hall effect (Zhang et al., 2005), its mechanical properties, such as Young's modulus: 1100 GPa and its resistance to fracture close to 125 GPa (Lee et al., 2008), and, finally, its large specific surface area of around 2630 m^2 g^{-1} (Chae et al., 2004).

Chemical exfoliation which consists on oxidation of graphite followed by exfoliation to graphene oxide (GO) and subsequent chemical reduction to reduced graphene oxide (rGO) is a common route for generating graphene based materials, because its low cost, since it requires relatively inexpensive equipment, and large quantity production. However, by using this method some oxygen functional groups remain and the defects partially disrupt the inherent sp^2 hybridized structure and morphology of graphene. Hence, rGO has not as good properties as monolayer graphene. On the contrary, the presence of remaining oxygen functional groups gives rGO a better dispersibility in most solvents. On the other hand, liquid phase exfoliation of pristine graphite produces high quality few-layer defect-free graphene (deG) but it presents poor dispersibility and low yield (mass of graphene product/mass of graphite feedstock). Typical yields reported in the literature for well dispersed pristine graphene nanosheets are <2% (Texter, 2015). CNTs can be prepared by three different methods: arc discharge, laser ablation, and chemical vapor deposition (Anzar et al., 2020). However, MWCNTs present an extremely poor solubility in water and other solvents, being a serious limitation for their practical applications (Kharissova et al., 2013).

Given its high hydrophobicity, the preparation of stable aqueous dispersions of carbonaceous materials requires the use of surfactants that promote the wetting tendency of the dispersions. It is necessary to utilize an appropriate amount of surfactant to obtain better dispersion and uniformity. Surfactant molecules can be absorbed on the surface of MWCNTs or graphene materials via hydrophobic interactions, π-π bonds, hydrogen bonds or electrostatic interactions which stabilize the distribution of the material in the solution (Keinanen et al., 2018). In addition, surfactants are intercalation agents, widening the distance between the graphite layers (Feng et al., 2020). These stable suspensions are able to be deposited in a large variety of substrates by the use of different deposition techniques, such as spray coating (Allen et al., 2010) or spin coating (Kymakis et al., 2011). These techniques allow producing conductive films with many applications in the fields of electronics and optoelectronics (Bonaccorso et al., 2010).

In a previous work we explored the possibility of preparing radionuclide sources on rGO-based thin films (Roteta et al., 2016). However this study was limited to rGO and no other carbon materials were evaluated. In addition, the best results were obtained for thin films prepared with rGO reduced by hydroiodic acid which is not an environmentally friendly reductant. In this work, readily available and cost-effective radioactive sources supported on carbonaceous thin films on VYNS are investigated as a suitable alternative to the conventional metallized films avoiding the shortcoming of the loss of many broken films of the high percentage of broken films. Graphene-based materials were prepared by both oxidation-exfoliation-reduction and direct graphite exfoliation routes. In addition, CNTs thin films were also evaluated. Since VYNS films are not resistant to the most common organic solvents used to stabilize graphene and MWCNTs dispersions (DMF, NMP, DMSO), the stabilization of graphene-based and CNTs aqueous dispersions was studied by using ionic (sodium dodecylbenzene sulfonate, SDBS) and non-ionic (Triton X-100) surfactants.

2. Materials and methods

2.1. Synthesis of graphene oxide

GO was synthesized following the guidelines given by the Tour method (Marcano et al., 2010). Briefly, 3 g of graphite powder were weighed together with 18 g of $KMnO_4$ and placed in a beaker. 400 mL of a mixture of concentrated H_2SO_4/H_3PO_4 (9:1 vol ratio) were added. The mixture was then stirred at 50 °C for 16 h, changing its color from dark purplish to dark brown. 400 mL of ice milliQ water and 10 mL of 30 % H_2O_2 were subsequently added in order to finish oxidation reaction resulting in a bright yellow suspension with bubbling. The suspension was decanted overnight and the supernatant removed and discarded. The remaining solid was filtered and washed successively, with 250 mL 10% v/v HCl and ultrapure water until pH of the supernatant achieved 6–6.5. Finally, the solid graphite oxide was freeze dried by lyophilization.

2.2. Synthesis of reduced graphene oxide

A combined hydrothermal-chemical reduction method was applied to reduce the GO. 300 mg of GO were dispersed in 60 mL of ultrapure water (5 mg mL^{-1}). The mixture was first sonicated using a Selecta ultrasonic bath for 1 h and subsequently with an ultrasonic probe (Bandelin Sonoplus HD 2070) for 1 h yielding homogenous brown GO dispersions. The resulting dispersions were transferred into PTFE-lined stainless steel autoclaves and subjected to 120 °C for 24 h. Obtained residues were transferred to a beaker and 6 g de L-ascorbic acid were added (100 mg mL^{-1}). The mixture was stirred for another 48 h. The obtained products were washed twice with ultrapure water and dried at 60 °C under vacuum. A final thermal annealing was performed at 400 °C during 24 h under Ar atmosphere. Finally, the as-obtained rGO was ground in an agate mortar.

2.3. Synthesis of carbon nanotubes

Catalytic decomposition of a gas-phase carbon source (acetylene) was used to synthesise multi-walled carbon nanotubes (MWCNTs) in a reactor consisting of a horizontal furnace and a quartz tube through which the reactants were introduced into the furnace at 1023 K. Iron pentacarbonyl ($Fe(CO)_5$) was used as the precursor for the iron catalyst

Table 1
Prepared dispersions of carbon-based materials.

Dispersion	Carbonaceous material	Concentration (mg.mL^{-1})	Surfactant
1	rGO	0.1	SDBS
2	rGO	0.1	Triton X-100
3	rGO	0.1	Sodium citrate
4	deG	10	SDBS
5	deG	10	Triton X-100
6	CNT	1	SDBS
7	CNT	1	Triton X-100

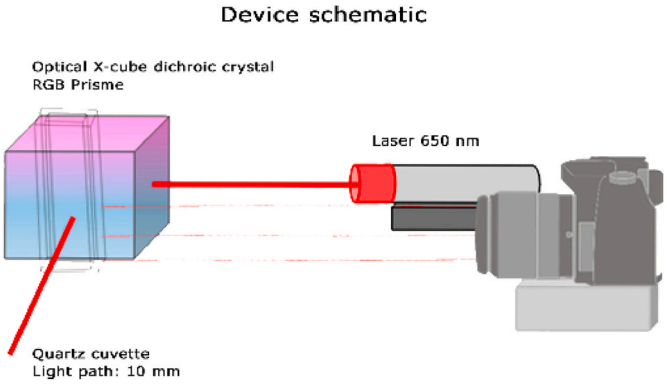

Fig. 1. Schematic device of the Tyndall effect tester.

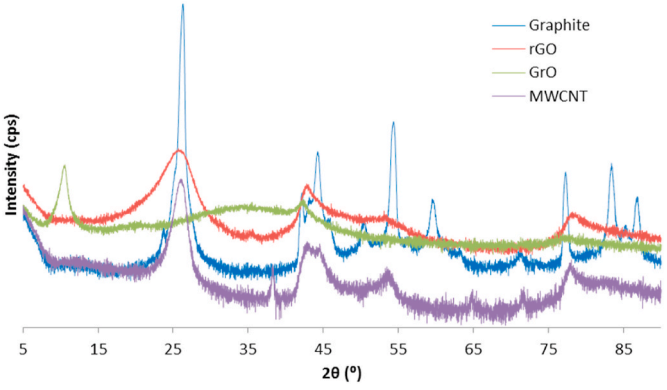

Fig. 2. XRD patterns of graphite and carbon-based synthesized materials.

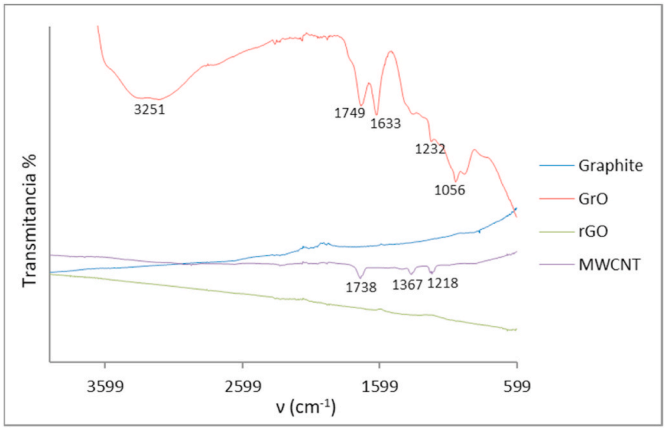

Fig. 3. FTIR spectra of graphite and carbon-based synthesized materials.

by bubbling nitrogen gas through the precursor solution in the reaction zone at 0 °C (Perez-Cadenas et al., 2012; Sampedro-Tejedor et al., 2007). A mixture of nitrogen and hydrogen was used, the former as carrier gas and the latter as reducing agent for the metal catalyst. $Fe(CO)_5$ was thermally decomposed in the tubular reactor to form iron nanoparticles on which MWCNTs were nucleated and grown. Quartz plates were placed in the centre of the reactor on which the formed nanotubes were deposited to facilitate their recovery, although the MWCNTs were also deposited on the walls of the quartz reactor tube. The material was recovered from all surfaces and subsequently characterized.

2.4. Preparation of aqueous dispersions

Aqueous dispersions of rGO, deG and CNT were prepared using different surfactants as it is given in Table 1. The suspensions were subjected to sonication with a probe sonicator for 2 h. In the case of deG dispersions, a centrifugation step was performed after sonication at 3000 rpm for 15 min to sediment unexfoliated graphite and the top supernatant containing few-layer graphene flakes was collected as the final graphene dispersion. SDBS, Triton X-100 and sodium citrate were added following optimal values from the literature (Giovannetti et al., 2016; Li et al., 2020; Wang and Zhang, 2019).

2.5. Preparation of carbon-based thin films supported on VYNS

VYNS films production method is similar to that described by Pate and Yaffe (1955). It is based on a drop-casting method where a drop of VYNS solution is cast on the surface of ultrapure water contained in a bath, which enables its expansion and polymerization. Subsequently, an aluminum ring is immersed in the solution to collect and hold the VYNS layer. The remaining polymer around the outer edge of the ring is cut manually using a scalpel. The film, mounted on the aluminum ring is dried at room temperature or under an infrared lamp. rGO, deG and CNT dispersions were spin-coated onto the VYNS substrates. Aluminum rings were placed over a polyethylene terephthalate (PET) substrate and fixed with Kapton tape so that they can be held by vacuum in a spin coater (CONVAC 1001). A drop of 1 mL of the corresponding dispersion was deposited onto the VYNS surface and a spinning program with a three-step profile comprising spin rates of 200 rpm for 10s, 500 rpm for 45s and 1000 rpm for 10s was used to coat the surface of the VYNS membrane without breaking it.

2.6. Characterization analysis

X-ray diffraction (XRD) patterns of all the samples were recorded on a Philips powder diffractometer PW3040/00 X'Pert MPD/MRD with Cu anode and a graphite secondary monochromator. The working conditions used included automatic slit divergence, 10 mm irradiated length, 10 mm mask, X'Celerator detector, 2.2 kW, voltage 45 kV, intensity 40 mA X-ray tube, 0.01° step size, 20 s time per step and applying a Cu-kα radiation ($\lambda = 0.15406$ nm) with a radius of 200 mm and an angle of 6°.

FT-IR analyses were performed by a spectrometer Varian Excalibur Series 3100. This instrument operates individually and it is equipped with a high resolution interferometer made up of a KBr beamsplitter, which allows working in the range from 7000 to 400 cm^{-1} with a spectral resolution from 32 to 0.09 cm^{-1}.

Scanning electron micrographs were recorded on a FEG-Nova Nano SEM 230 Field Emission Electron Microscope, equipped with a ELD detector (Everhart-Thornley Detector) for secondary electrons. Prior to analysis, samples were metallized by gold coating using the sputter-coater deposition method, in which a thin film is subjected to ionic bombardment of gold. This treatment was performed using a BALTEC (Leica) EM ACE600 equipment.

The nature of the prepared dispersions was studied by a typical experiment conducted in colloid science called the Tyndall effect. This experiment was carried out using a LEICA EM ACE200 camera and close-

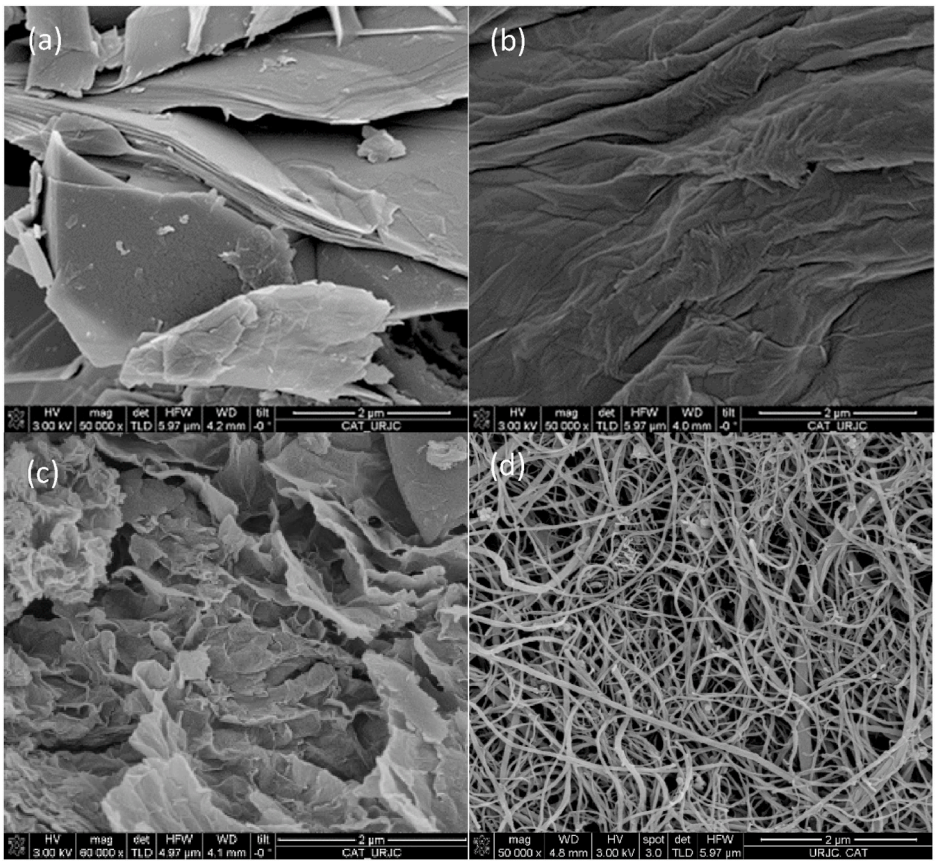

Fig. 4. SEM images of graphite and carbon-based synthesized materials (a) graphite, (b) GO, (c) rGO, (d) MWCNT.

up lenses that allow surface details to be enlarged up to 10 times. Images taken in appropriate lighting conditions have a resolution of 4608 x 3072 pixels. A device was designed in which light from a laser pointer with wavelength of 650 nm passed through an optical X-cube dichroic crystal RGB prism, striking a quartz cuvette with a light path (10 mm). The used device allows perpendicular incidence of light of laser across the cuvette of quartz (Fig. 1).

2.7. Measurement of radiolabeled sources

The aqueous dispersions described in Table 1 were used to prepare a series of VYNS films with different types of carbon materials. Each type of film was used for the production of radioactive sources by drop deposition and simple evaporation of ^{55}Fe. The energy resolution was analyzed with all of them and the results obtained with the VYNS films plated with Au–Pd were compared. Sources containing ^{55}Fe, emitting low energy electrons, allow checking the spectrometric quality in the low energy region and determining the energy resolution of the 5–6.5 keV Auger electron peaks. In all cases, sources were measured on a 4π Pressurized Proportional Counter (PPC). The system is pressurized with PR gas (a mixture of 90% argon and 10% methane) at 750 kPa. In this detector, it is required that the radioactive samples be deposited on a conductive support since the electrically charged particles are emitted by the sample and the emission of charged particles will leave the sample charged. If the support were not conductive, some of the pulses could be too small and the spectrum could be degraded because the electric field does not remain constant in the vicinity of the sample. The situation is particularly unfavorable when measuring electron emitters with 4π PPCs because the charge created in the avalanche could not be neutralized and could affect the following electron emissions, especially if they are of low energy, reducing the quality of the spectrum. Therefore, samples measured in this device are usually metallized with Au–Pd alloys, a material with high atomic number that can cause attenuation of charged particles and gamma radiation. The use of carbon materials aims to produce low atomic number conductive samples.

3. Results and discussion

3.1. Characterization

X-ray diffraction patterns of graphite, GrO, rGO and MWCNTs are shown in Fig. 2. The 2θ diffraction peak of GO appeared to be 10.62°, corresponding to d_{001} plane, confirmed the oxidation of the graphitic structure and the formation of oxygenated functional groups such as carbonyl, carboxyl, epoxide and hydroxyl groups in graphite oxide, with an obvious disappearance of graphite characteristic peaks, indicating a new lattice structure which is significantly different from the pristine graphite (Kartick et al., 2013). Following chemical and thermal exfoliation and reduction, in the XRD pattern of rGO the (001) band completely disappears due to the partial removal of oxygen groups. On the contrary, XRD pattern was similar to that of graphite showing a typical peak at $2\theta = 25.80^{\circ}$, indicating the progressive reconstruction of the crystalline structure (Muzyka et al., 2018). The peak, however, was rather broad, which might be attributed to very thin graphene layers due to high degree of exfoliation. This result indicated that the graphene nanosheets were exfoliated into few-layers. The interlayer distance is significantly lower than the corresponding for GO which implies that most of the functional groups were removed (Meng and Park, 2012). However the higher basal spacing with respect to the theoretical value (0.335 nm) (Wu et al., 2020) may be related to the presence of significant amounts of oxygen in the rGO and a large degree of defect formation in the graphene layers due to the incomplete reduction of GO sheets which is typical from rGO obtained by the chemical route (Chua and Pumera, 2014). The XRD results obtained for MWCNTs presented two

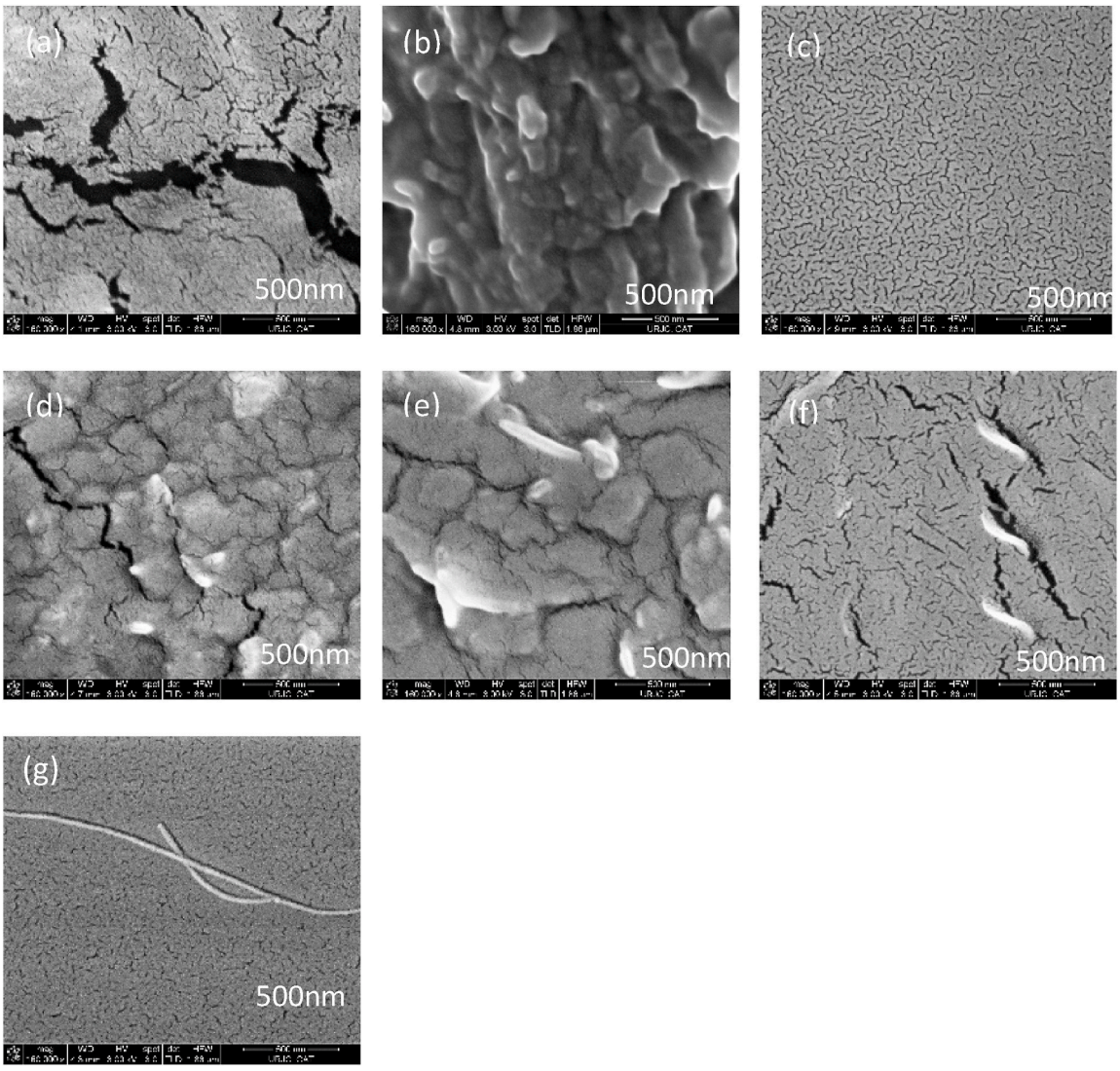

Fig. 5. SEM images of carbon-based materials thin films. (a) Dispersion 1, (b) dispersion 2, (c) dispersion 3, (d) dispersion 4, (e) dispersion 5 (f) dispersion 6 and (g) dispersion 7.

peaks at 26.45° and 44.57° which are typical from CNTs (Arunkumar et al., 2020). These peaks show the presence of carbon in the product and also the hexagonal structure. Other peaks at 38.30°, 44.57°, 64.78°, 71,80°, 77.90° belong to the catalysis used for the synthesis of the MWCNTs. The crystalline size of the sample was determined using Scherrer Equation (1), which is 39.49 nm and lattice strain was 0.6661.

$$D_p = \frac{0.94\lambda}{\beta_{1/2}\cos\theta} \quad (1)$$

Fig. 3 shows the FTIR spectra of GO and rGO, together with those of graphite and MWCNT. The GO spectrum shows a peak at 1056 cm^{-1} attributed as *C*–O stretching. The peak at 1232 cm^{-1} is confirmed as *C*–*O*–C bending and aromatic C═C stretching is observed at 1633 cm^{-1}. The carbonyl groups are also shown at 1749 cm^{-1} as C═O stretching and a broad peak at 3251 cm^{-1} is attributed as O–H stretching vibration of the *C*–OH groups and water content in the material. These peaks do not appear in the FTIR spectrum of graphite, indicating that the oxidation process through the Tour method introduced a large number of oxygen-containing functional groups, including –COOH and C═O located at the sheet edge as well as –OH and epoxy *C*–O on the basal planes of the GO sheet (Stankovich et al., 2006). The curve of rGO was similar to that of graphite, showing the restoration of electronic conjugation within graphene sheets. The rGO spectrum confirms the reduction of oxygen-containing groups on GO by the combined ascorbic acid (L-AA) and thermal process. The peaks at 1056, 1232 and 1749, 3251 cm^{-1} disappeared and decreased dramatically, this is an indication of the removal of oxygen-containing functional groups in GO to a high degree. Considering this result, it can be deduced that the combination of chemical reduction by L-AA and final thermal annealing constitutes a highly effective route to reduce GO leading to a high quality rGO. The very poor transmittance of graphite, rGO and MWCNT samples can be due to the strong absorption of the infrared light by these materials (Eo et al., 2008) and the low number of surface groups.

SEM images of graphite and carbon-based synthesized materials are depicted in Fig. 4. Graphite flakes (Fig. 4a) show a laminar morphology with an ordered layer structure (Arduini et al., 2010). In contrast, GO (Fig. 4b) reveals a typical randomly aggregated, thin, crumpled flake structure (Aliyev et al., 2019). It exhibits that the oriented layer structure of graphite has been unbalanced due to its oxidation. SEM image of rGO (Fig. 4c) shows an oriented structure as randomly crumpled silk veil waves. The nanosheets are rippled and entangled with each other. The lamella structure of wrinkled rGO nanosheets is due to the van der Waals interactions (Saleem et al., 2018). SEM image of the nanotubes grown (Fig. 4d) shows aligned MWCNTs not associated in bundles (Castillejos et al., 2012; Sampedro-Tejedor et al., 2007), where the bright points

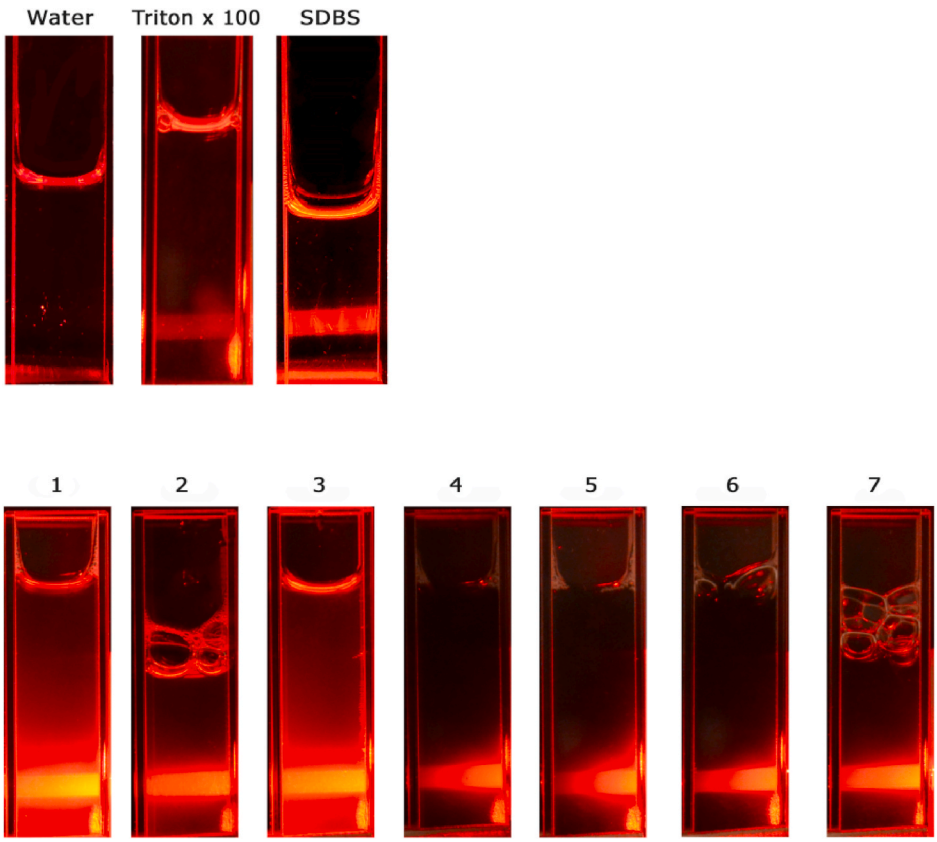

Fig. 6. Images of Tyndall effect in aqueous dispersions of the surfactants and carbon-based materials used in this study. (1) dispersion 1, (2) dispersion 2, (3) dispersion 3, (4) dispersion 4, (5) dispersion 5 (6) dispersion 6 and (7) dispersion 7.

correspond to the $Fe(CO)_5$ used as catalyst (Shivashankar and Arod, 2015).

Fig. 5 presents SEM images of thin films from the different prepared dispersions deposited on glass slides. In the case of dispersions 1 and 3, Fig. 5a and c, respectively, clearly show dense and uniform graphene flakes with homogeneously smooth and wavelike sheet morphology throughout the film. For the rest of graphene dispersions (Fig. 5b, d and 5e), SEM images display a more flake-like microstructure with overlapping adjacent graphene nanoplatelets clearly distinguishable (Hu et al., 2017). For MWCNT thin films (Fig. 5f and g), the carbonaceous material appears embedded with the surfactant. In addition, since only a few MWCNTs are distinguishable, it is evident that a complete disruption of the MWCNT structure also occurs as a consequence of sonication process. Some authors have reported that extended grinding have a low impact on the MWCNT properties and even an improvement on the specific surface is observed (Batmunkh et al., 2012).

All diluted rGO dispersions gave rise the Tyndall effect confirming its colloidal nature (Li et al., 2008). In Fig. 6 it is observed that dispersions 1, 2 and 3 have a greater range of light scattering. It may be due to spread produced by GO previously reduced, causing the surfactant adsorb in a non-homogeneous way between the rGO sheets.

3.2. Discussion of the measurement of the radiolabeled sources

Sources of the radionuclide ^{55}Fe, which is often used as a reference radionuclide at low energies and emits X-rays in the interval from 5 to 6.5 keV, were prepared by deposition of a drop of their respective solutions on the prepared thin films. An additional source prepared using conventional Au–Pd coated VYNS foil was also fabricated for comparison purposes. The emission probabilities are taken from the Atomic and Nuclear Data recommended by the LNHB ((LNHB), 2021).

^{55}Fe disintegrates by electron capture mainly to the ground state of ^{55}Mn. In its relaxation process, manganese emits X-rays of approximately 5.9 keV (k_α) with a probability of 25.02 % and 6.5 keV (k_β) with a probability of 3.4 %. Along with the X-rays, Auger electrons between 4.9 and 6.5 keV are emitted with a probability of 60 %.

It can be seen in Fig. 7 that the main peak of most spectra present a smooth shape, close to a gaussian curve but, as expected, slightly less steep to the right, as a consequence of the small contribution of k_β, which is too close to k_α to be resolved in a gas-filled detector. The resolution is very similar for all tested sources, being higher than 0.9 keV which is typical for spectra obtained with Ar/CH_4 proportional counters (Elvira et al., 2020).

All of them show a prominent main peak, corresponding to the contribution of both low energy electrons and photons in the 5–6.5 keV range from ^{55}Fe (Atomic and Nuclear Data), which means that all of them present enough conductivity to detect low-energy electrons. The lower energy peak to the left of the main one is due to the escape of photon X-rays from argon and are in the range of 3 keV. Among the displayed spectra in Fig. 7, rGO-Triton X-100 presents a spectrum with an energy resolution comparable with that of the metallized source (Au–Pd) and with a distinguishable and clean escape peak. In all films the main peak is observable and clearly separated from the escape peak. Although in cases rGO-SDBS, deG-SDBS and deG-Triton X-100, the intensity of the escape peak is similar to the rGO-triton X-100 this is not as clean as that in rGO-Triton X-100. The better performance of rGO-based thin films can be attributed to the residual oxygen groups in their structure that enhance the interaction with the surfactant. The heterogeneity of rGO sheets with areas of pure graphene of a few nanometers in lateral size interleaved with heavily oxidized regions, where the residual oxygen functional (mostly hydroxyl and epoxy) groups characteristic of rGO are concentrated, results in more intense interaction between the rGO and the surfactant molecules (Erickson et al., 2010; Gomez-Navarro et al., 2010; Zhang et al., 2013). However, several sources, specifically

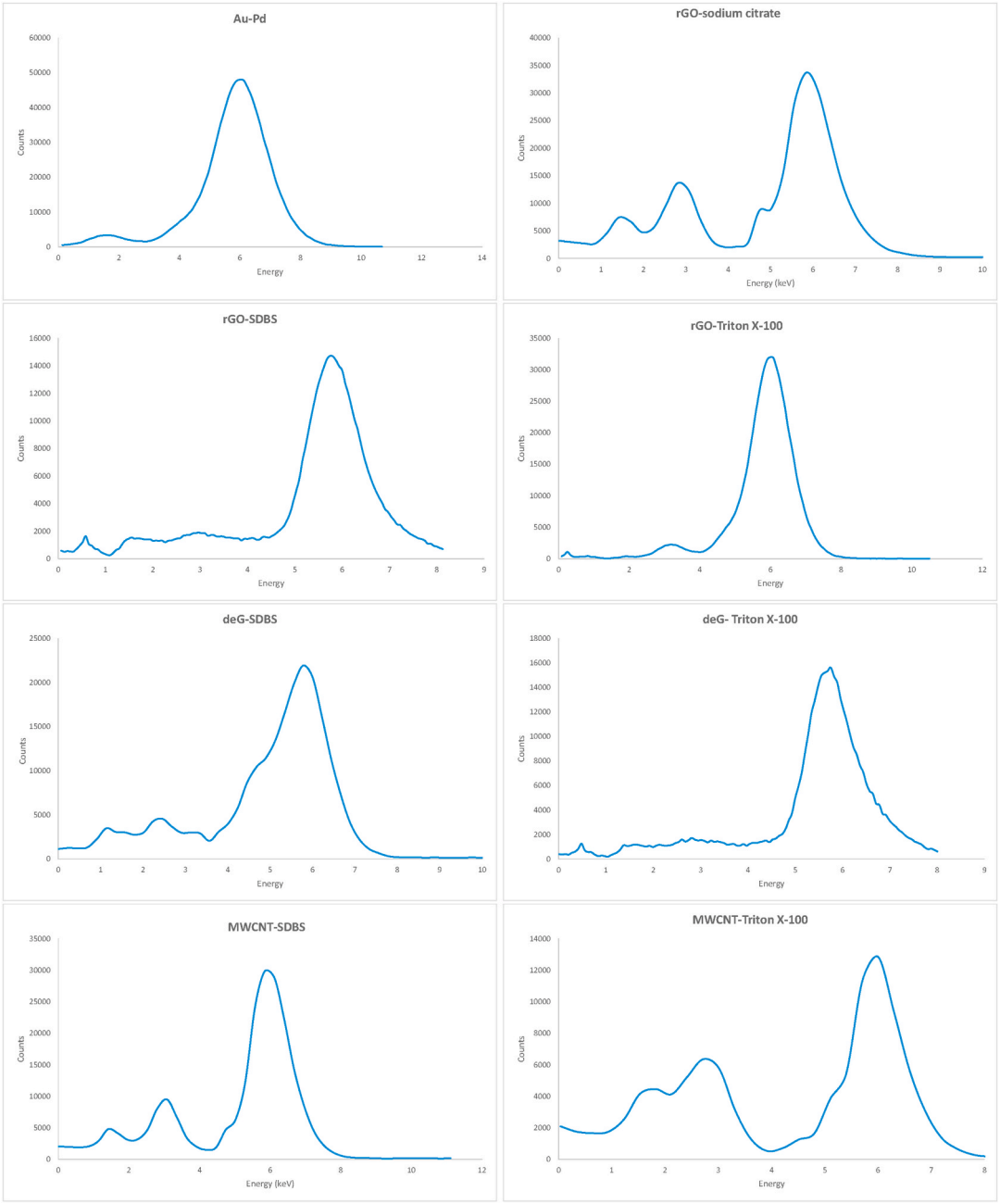

Fig. 7. X-ray spectra of 55Fe measured with the proportional counter in the carbon-based thin films compared with a conventional Au–Pd coated source.

rGO-sodium citrate, MWCNT-SDBS and MWCNT-Triton X-100, present escape peaks and low energy tails to the origin of the spectrum with excessive relative intensities, maybe due to the lack of conductivity of the support. In conclusion, the quality obtained with rGO-Triton X-100 is similar to that of the metallized sample.

4. Conclusions

Carbon-based thin films have been prepared as conductive support for radionuclide labeling in the range of low energy. Thin films were prepared by spin coating aqueous solutions of rGO, deG and MWCNTs on VYNS films. Homogeneous dispersions could be achieved by using both ionic and non-ionic surfactants. Characterization analysis of GO and rGO confirmed the oxidation of graphite in a large extent as well as the restoration of conjugated structure by the subsequent reduction process. SEM micrographs of prepared thin films showed a large heterogeneity in the rGO films which in turn yielded the ^{55}Fe spectra with the best characteristics. From the obtained spectra, we can conclude that MWCNT dispersions are not suitable to prepare radioactive sources for the measurement of low-energy electrons due to the high intensity of the escape peaks. Similarly, the absence of surfactant is not advisable. On the contrary, sources prepared with graphene-based materials such as rGO and deG showed spectra comparable to the metallized sources. Among them, rGO-Triton X-100 presented a high quality spectrum with a resolution and escape peak similar to that of a conventional Au–Pd metallized source. The present work showed that it is possible to fabricate radioactive sources at low energy levels by means of graphene-based thin films prepared from aqueous dispersions yielding spectra of quality similar to those prepared by metallization procedure avoiding the use of expensive Au–Pd solutions and without the problem of breakage of metallized rings.

CRediT authorship contribution statement

Rodolfo Fernández-Martínez: Conceptualization, Data curation, Methodology, Supervision, Writing – original draft, Writing – review & editing. **M[a] Isabel Rodríguez-Tapiador:** Writing – original draft, Methodology, Formal analysis. **Miguel Roteta:** Writing – original draft, Supervision, Software. **María Pérez-Cadenas:** Writing – review & editing, Supervision, Resources, Methodology. **Gilberto del Rosario:** Methodology. **Jorge Pedrós:** Writing – review & editing, Resources, Methodology. **Isabel Rucandio:** Writing – review & editing, Supervision, Funding acquisition, Conceptualization.

Declaration of competing interest

The authors declare that they have no known competing financial interests or personal relationships that could have appeared to influence the work reported in this paper.

None.

Data availability

Data will be made available on request.

Acknowledgments

Grants ENE2017-88065-C2-2-R funded by MCIN/AEI/10.13039/501100011033 and by ERDF A way of making Europe and PID2020-114234RB-C21 funded by MCIN/AEI/10.13039/501100011033. J.P. acknowledges financial support from the Spanish Ministry of Science & Innovation through project 2D-SAWNICS (PID2020-120433 GB-I00) and from Comunidad de Madrid through project NMAT2DCM (P2018/NMT-4511).

References

Aliyev, E., Filiz, V., Khan, M.M., Lee, Y.J., Abetz, C., Abetz, V., 2019. Structural characterization of graphene oxide: surface functional groups and fractionated oxidative debris. Nanomaterials 9, 1180.

Allen, M.J., Tung, V.C., Kaner, R.B., 2010. Honeycomb carbon: a review of graphene. Chem. Rev. 110, 132–145.

Anzar, N., Hasan, R., Tyagi, M., Yadav, N., Narang, J., 2020. Carbon nanotube - a review on Synthesis, Properties and plethora of applications in the field of biomedical science. Sensors International 1, 100003.

Arduini, F., Giorgio, F.D., Amine, A., Cataldo, F., Moscone, D., Palleschi, G., 2010. Electroanalytical characterization of carbon black nanomaterial paste electrode: development of highly sensitive tyrosinase biosensor for catechol detection. Anal. Lett. 43, 1688–1702.

Arunkumar, T., Karthikeyan, R., Ram Subramani, R., Viswanathan, K., Anish, M., 2020. Synthesis and characterisation of multi-walled carbon nanotubes (MWCNTs). Int. J. Ambient Energy 41, 452–456.

Balandin, A.A., 2011. Thermal properties of graphene and nanostructured carbon materials. Nat. Mater. 10, 569–581.

Batmunkh, M., Bayaraa, N., Rehman, H., Kim, J., Chung, H., Jeong, H., 2012. Grinding characteristic of multi-walled carbon nanotubes-alumina composite particle. J. Wuhan Univ. Technol.-Materials Sci. Ed. 27.

Bonaccorso, F., Sun, Z., Hasan, T., Ferrari, A.C., 2010. Graphene photonics and optoelectronics. Nat. Photonics 4, 611–622.

Castillejos, E., Bachiller-Baeza, B., Pérez-Cadenas, M., Gallegos-Suarez, E., Rodríguez-Ramos, I., Guerrero-Ruiz, A., Tamargo-Martinez, K., Martinez-Alonso, A., Tascón, J. M.D., 2012. Structural and surface modifications of carbon nanotubes when submitted to high temperature annealing treatments. J. Alloys Compd. 536, S460–S463.

Chae, H.K., Siberio-Perez, D.Y., Kim, J., Go, Y., Eddaoudi, M., Matzger, A.J., O'Keeffe, M., Yaghi, O.M., 2004. A route to high surface area, porosity and inclusion of large molecules in crystals. Nature 427, 523–527.

Chua, C.K., Pumera, M., 2014. Chemical reduction of graphene oxide: a synthetic chemistry viewpoint. Chem. Soc. Rev. 43, 291–312.

deSanoit, J., Geffroy, B., Rosilio, C., Hainos, D., 1997. A new conducting polymer radioactive source support for 4 pi beta-gamma coincidence counting. Nucl. Instrum. Methods Phys. Res. Sect. B Beam Interact. Mater. Atoms 131, 305–312.

Du, H.S., Liu, Y.P., Li, J.L., Yan, S.J., Li, G.H., Zhu, Y., Yao, L.N., 1996. Progress in preparation 4 pi beta quantitative sources. Nucl. Instrum. Methods Phys. Res. Sect. A Accel. Spectrom. Detect. Assoc. Equip. 369, 424–426.

Elvira, V.H., Peyres, V., Roteta, M., Fernandez-Sotillo, A., Garcia-Torano, E., 2020. Absolute determination of low-energy X-ray emission rates with a proportional counter. Appl. Radiat. Isot. 160.

Eo, S.M., Oh, S.J., Tan, L.S., Baek, J.B., 2008. Poly(2,5-benzoxazole)/carbon nanotube composites via in situ polymerization of 3-amino-4-hydroxybenzoic acid hydrochloride in a mild poly(phosphoric acid). Eur. Polym. J. 44, 1603–1612.

Erickson, K., Erni, R., Lee, Z., Alem, N., Gannett, W., Zettl, A., 2010. Determination of the local chemical structure of graphene oxide and reduced graphene oxide. Adv. Mater. 22, 4467–4472.

Feng, B.-B., Wang, Z.-H., Suo, W.-H., Wang, Y., Wen, J.-C., Li, Y.-F., Suo, H.-L., Liu, M., Ma, L., 2020. Performance of graphene dispersion by using mixed surfactants. Mater. Res. Express 7.

Geim, A.K., Novoselov, K.S., 2007. The rise of graphene. Nat. Mater. 6, 183–191.

Giovannetti, R., Rommozzi, E., Zannotti, M., D'Amato, C.A., Ferraro, S., Cespi, M., Bonacucina, G., Minicucci, M., Di Cicco, A., 2016. Exfoliation of graphite into graphene in aqueous solution: an application as graphene/TiO2 nanocomposite to improve visible light photocatalytic activity. RSC Adv. 6, 93048–93055.

Gomez-Navarro, C., Meyer, J.C., Sundaram, R.S., Chuvilin, A., Kurasch, S., Burghard, M., Kern, K., Kaiser, U., 2010. Atomic structure of reduced graphene oxide. Nano Lett. 10, 1144–1148.

Hu, M.C., Yao, Z.H., Wang, X.Q., 2017. Characterization techniques for graphene-based materials in catalysis. AIMS Mater. Sci. 4, 755–788.

Kartick, B., Srivastava, S.K., Srivastava, I., 2013. Green synthesis of graphene. J. Nanosci. Nanotechnol. 13, 4320–4324.

Keinanen, P., Siljander, S., Koivula, M., Sethi, J., Sarlin, E., Vuorinen, J., Kanerva, M., 2018. Optimized dispersion quality of aqueous carbon nanotube colloids as a function of sonochemical yield and surfactant/CNT ratio. Heliyon 4, e00787.

Kharissova, O.V., Kharisov, B.I., de Casas Ortiz, E.G., 2013. Dispersion of carbon nanotubes in water and non-aqueous solvents. RSC Adv. 3, 24812–24852.

Kymakis, E., Stratakis, E., Stylianakis, M.M., Koudoumas, E., Fotakis, C., 2011. Spin coated graphene films as the transparent electrode in organic photovoltaic devices. Thin Solid Films 520, 1238–1241.

Lee, C., Wei, X.D., Kysar, J.W., Hone, J., 2008. Measurement of the elastic properties and intrinsic strength of monolayer graphene. Science 321, 385–388.

Li, D., Müller, M.B., Gilje, S., Kaner, R.B., Wallace, G.G., 2008. Processable aqueous dispersions of graphene nanosheets. Nat. Nanotechnol. 3, 101–105.

Li, L., Zhou, M., Jin, L., Mo, Y., Xu, E., Chen, H., Liu, L., Wang, M., Chen, X., Zhu, H., 2020. Green preparation of aqueous graphene dispersion and study on its dispersion stability. Materials.

Liu, P., Zhou, D., Zhang, C., Wei, H., Yang, X., Wu, Y., Li, Q., Liu, C., Du, B., Liu, L., Jiang, K., Fan, S., 2018. Crystalline multiwall carbon nanotubes and their application as a field emission electron source. Nanotechnology 29, 345601.

(LNHB), L.N.H.B., 2021. Atomic and nuclear Data. http://www.lnhb.fr/nuclear-data/nuclear-data-table.

Lowenthal, G.C.S.A.M., 1964. Use of Au-20% Pd for metallising thin source supports for 4π proportional gas flow counters. Nucl. Instrum. Methods 30, 363–364.

Marcano, D.C., Kosynkin, D.V., Berlin, J.M., Sinitskii, A., Sun, Z.Z., Slesarev, A., Alemany, L.B., Lu, W., Tour, J.M., 2010. Improved synthesis of graphene oxide. ACS Nano 4, 4806–4814.

Meng, L.Y., Park, S.J., 2012. Preparation and characterization of reduced graphene nanosheets via pre-exfoliation of graphite flakes. Bull. Kor. Chem. Soc. 33, 209–214.

Moura, L.P., Parker, W.C., 1975. Effect of thin film resistance variation on the absolute standardization of radionuclides. Nucl. Instrum. Methods 129, 565–568.

Muzyka, R., Drewniak, S., Pustelny, T., Chrubasik, M., Gryglewicz, G., 2018. Characterization of graphite oxide and reduced graphene oxide obtained from different graphite precursors and oxidized by different methods using Raman spectroscopy. Materials 11, 15.

Nair, R.R., Blake, P., Grigorenko, A.N., Novoselov, K.S., Booth, T.J., Stauber, T., Peres, N. M.R., Geim, A.K., 2008. Fine structure constant defines visual transparency of graphene. Science 320, 1308, 1308.

Novoselov, K.S., Geim, A.K., Morozov, S.V., Jiang, D., Zhang, Y., Dubonos, S.V., Grigorieva, I.V., Firsov, A.A., 2004. Electric field effect in atomically thin carbon films. Science 306, 666–669.

Pate, B.D., Yaffe, L., 1955. A new material and techniques for the fabrication and measurement of very thin films for use in 4πβ-γ counting. Can. J. Chem. 33, 15–23.

Perez-Cadenas, M., Munoz-Andres, V., Rodriguez-Ramos, I., Maroto-Valiente, A., Guerrero-Ruiz, A., 2012. Building up multiwall carbon nanotubes nanostructures inside millimetric channels of ceramic monoliths. J. Nano Res. 18–19, 271–279.

Roteta, M., Fernandez-Martinez, R., Mejuto, M., Rucandio, I., 2016. Preparation of graphene thin films for radioactive samples. Appl. Radiat. Isot. 109, 217–221.

Saleem, H., Haneef, M., Abbasi, H.Y., 2018. Synthesis route of reduced graphene oxide via thermal reduction of chemically exfoliated graphene oxide. Mater. Chem. Phys. 204, 1–7.

Sampedro-Tejedor, P., Maroto-Valiente, A., Nevskaia, D.M., Munoz, V., Rodriguez-Ramos, I., Guerrero-Ruiz, A., 2007. The effect of growth temperature and iron precursor on the synthesis of high purity carbon nanotubes. Diam. Relat. Mater. 16, 542–549.

Shivashankar, S., Arod, P., 2015. Single-step synthesis of Carbon Nanotubes/Iron/Iron oxide composite films through inert-ambient CVD using ferric acetylacetonate as precursor. RSC Adv. 5.

Sibbens, G., Altzitzoglou, T., 2007. Preparation of radioactive sources for radionuclide metrology. Metrologia 44, S71–S78.

Sonkar, P., Kumar, N., Gupta, P., 2021. Characteristics of Carbon Nanotubes and Their Nanocomposites, pp. 99–118.

Stankovich, S., Dikin, D.A., Dommett, G.H.B., Kohlhaas, K.M., Zimney, E.J., Stach, E.A., Piner, R.D., Nguyen, S.T., Ruoff, R.S., 2006. Graphene-based composite materials. Nature 442, 282–286.
Texter, J., 2015. Colloidal graphene-Scalable processing for advanced materials. Curr. Opin. Colloid Interface Sci. 20, 305–310.
Wang, X., Zhang, L., 2019. Green and facile production of high-quality graphene from graphite by the combination of hydroxyl radicals and electrical exfoliation in different electrolyte systems. RSC Adv. 9, 3693–3703.
Wu, Y., Wang, S., Komvopoulos, K., 2020. A review of graphene synthesis by indirect and direct deposition methods. J. Mater. Res. 35, 76–89.
Yaffe, L., 1962. Preparation of thin films, sources, and targets. Annu. Rev. Nucl. Sci. 12, 153–188.
Zhang, Y.B., Tan, Y.W., Stormer, H.L., Kim, P., 2005. Experimental observation of the quantum Hall effect and Berry's phase in graphene. Nature 438, 201–204.
Zhang, Q., Zheng, H.J., Geng, Z.G., Jiang, S.L., Ge, J., Fan, K.L., Duan, S., Chen, Y., Wang, X.P., Luo, Y., 2013. The realistic domain structure of as-synthesized graphene oxide from ultrafast spectroscopy. J. Am. Chem. Soc. 135, 12468–12474.